Hindawi
Journal of Spectroscopy
Volume 2019, Article ID 6470601, 5 pages
https://doi.org/10.1155/2019/6470601

Research Article

The Effect of Cu Doping on the Transformation from Rutile to Anatase and Cu Occupation Tendency in TiO_2 Solid Solution

Jun-Yu Chen, Ji-Kang Yan, and Guo-You Gan

Kunming University of Science and Technology, Kunming, China

Correspondence should be addressed to Ji-Kang Yan; scyjk@qq.com

Received 27 September 2018; Accepted 23 January 2019; Published 14 February 2019

Academic Editor: Damien Boyer

TiO_2 doped with different amounts of Cu^{2+} ions (from 0 to 3 mol%) was synthesized by sol-gel method. The samples were characterized by X-ray diffraction (XRD) and Fourier-transform infrared spectroscopy (FTIR). The XRD analysis showed that the Cu-doped TiO_2 samples exhibit anatase and rutile phases. The lattice parameters remain unchanged, independent of Cu^{2+} content. Diameter of TiO_2 increased significantly with increasing concentrations of Cu^{2+}. The investigated results indicate that a greater portion of the Cu^{2+} ions are well incorporated into the anatase and rutile TiO_2 lattices. The stretching vibration frequencies of the interatomic bonds were calculated by the electronegativity principle. The calculated data were compared with infrared spectra. The results show that in the rutile and anatase phases, O atoms in the TiO_2 lattice and some interstitial Cu atoms form Cu-O bond, and other substitutional Cu that replaces Ti atoms in TiO_2 lattice form Cu-O bond with O atoms in the TiO_2 lattice.

1. Introduction

Titanium dioxide (TiO_2) is widely concerned with its cheapness, stability, environmental friendliness, and photocatalytic properties [1]. TiO_2 application is encircled as a photocatalyst in heterogeneous catalysis, or the production of hydrogen and electric energy in solar cells, as white pigments for cosmetic and paint industries, as a gas transducer, as a sunscreen cosmetic, as an edible pigment, in electronic equipment, in ceramics, and others [2]. However, undesired recombination of photoexcited carriers and wide band gap (3.2 eV) severely limits its practical application. One key challenge is to develop catalysts with high catalytic capability. Doping modification is found to play an important role for the catalytic performance of TiO_2. The photocatalytic activity of TiO_2 could be obviously improved by doping Cu, N, S, Fe, C, etc. [3]. In particular, doping of metals seems to be an effective way. Another approach to change the physical, optical, structural, and photocatalytic properties of titania includes an employment of d-block metal ions (zinc, zirconium, iron, chromium, nickel, vanadium, or copper) [4].

Recently, Cu doping has been increasingly investigated as a dopant for titania. The origin of the ferromagnetic property was explained based on the concentration of oxygen vacancies increased by Cu doping [5]. From the structural and surface analysis of the catalysts, we have stated that the occurrence of highly disperse and reducible Cu^{2+} species is directly related to the photocatalytic activity for the H_2 production reaction [6]. At present, we have no information about the doping position of Cu^{2+} ions that were researched [7]. Cu could replace Ti in the substitutional sites or be incorporated in the interstitial sites. In some cases, they may segregate on the surface [8]. The doping position of Cu can be calculated by the electronegativity principle [9]. Different doping positions of Cu atoms have an effect on the properties of particle, electron structure, and light absorption. In conclusion, there is a need to analyze the doped position of Cu, which will help understand in detail the role of the dopant in altering TiO_2 properties [10].

In this work, Cu-doped and undoped TiO_2 nanomaterials were prepared with the sol-gel method. The crystalline phase and IR spectra of the samples were characterized with X-ray diffraction and Fourier-transform infrared spectroscopy (FTIR). The objectives/goals of this study were to illustrate the Cu doping position that could be simulated by the electronegativity principle.

2. Experimental Details

2.1. Sample Preparation. The TiO_2 system was prepared by a sol-gel method using tetrabutyl titanate as a precursor (10 ml TBT) in water/ethanol solution (200 ml ethanol and 2 ml H_2O). Forced hydrolysis of the TBT solution was achieved by adding certain volume of bidistilled water (8.4 ml). The sol-gel synthesis in acidic solution was performed by substituting the initial 2 ml of water by the same volume of nitric acid (1 M). On the other hand, the copper-doped systems were obtaining by adding the 25 ml of $Cu(NO_3)_2{\cdot}3H_2O$. Doped and undoped TiO_2 systems were calcined in air at 550°C for 3~5 h.

2.2. Experiment Principles. The IR (photons or energy) absorption of molecules causes the vibration of each chemical bond in the molecule. The bond vibrations are similar to diatomic vibrations [11]. The reduced mass μ can be expressed as follows:

$$\frac{1}{\mu} = \frac{1}{m_1} + \frac{1}{m_2} = \frac{m_1 + m_2}{m_1 m_2}, \quad (1)$$

where m_1 and m_2 are the masses of the two bonded atoms ($m_{Ti} = 47.87$; $m_{Cu} = 55.845$; $m_O = 16.00$). The most mature theory for the vibrational ground state IR model is the harmonic oscillator model. According to classical mechanics, the stretching force constant k and frequency v satisfy the following relation [12]:

$$v = \frac{1}{2\pi}\sqrt{\frac{k}{\mu}}. \quad (2)$$

In Equation (2), the unit of v is cm^{-1}. At the same time, Yang et al. [13] proposed the following relationship between the force constants and electronegativity:

$$k = mN\left(\frac{XaXb}{d^2}\right)^{3/4} + n, \quad (3)$$

where k is the stretching force constant, d is the bond length, N is the bond order, and Xa and Xb are the electronegativities of the atoms at both ends of the bond (k unit: dynes/cm10−5; d unit: Å). The values of m and n are 1.67 and 0.30, respectively (for stable molecules and stably covalent atoms) [14]. The bond order N can be calculated as follows: N = (total number of electrons in a stable structure-total number of valence electrons)/2; the calculation yields a bond order of 0.5. By looking up the electronegativity table, the following values are obtained: XTi = 1.54, XO = 3.44, and XCu = 1.90 [14].

2.3. TiO_2 Molecular Structure Model. Figure 1 is the structural model of TiO_2. From the periodic arrangement, it can be seen that it constitutes multiple oxygen octahedral structure units, and so only the model of a single cell structure needs to be discussed. The basic unit in the structure of both rutile and anatase TiO_2 is oxygen octahedral. The subscript of element symbol represents the position of this atom. The number between the two atoms represents the bond length between the two atoms. For instance, Ti_A representing Ti atom is in titanium lattices of anatase TiO_2.

2.4. Cu-Doped TiO_2 Structure Model. Figures 2(a) and 2(b) show that in the anatase, Cu replaces Ti atoms in the substitutional sites or occupy in the interstitial sites. Figures 2(c) and 2(d) show that, in the anatase, Cu replaces Ti atoms in the substitutional sites or occupy in the interstitial sites. Doping substitutional and interstitial sites were constructed by using SDD configuration, GaussView, and Gaussian09w. The information of bond length and the position of each atom are shown in Figure 2. The dashed line between Cu and O indicates that Cu can form Cu_2O with two O atoms and can also form CuO with only an O atom. The lower right corner of the symbol indicated the atomic location number. The numbers between two atoms indicated the bond distance between two atoms (unit: Å).

2.5. Phase Analysis. Figure 3 can be seen that all samples show anatase and rutile phase regardless of Cu^{2+} content. The lattice parameters of samples calculated from the XRD patterns are shown in Table 1. The lattice parameters remain unchanged, independent on Cu^{2+} content. This is evident considering that a greater portion of the Cu^{2+} ions is well incorporated into the anatase and rutile TiO_2 lattice. When comparing to bulk anatase and rutile TiO_2, a small change in lattice constant has been observed for the Cu-doped TiO_2 samples as shown in Table 1. The reason for this may be due to the tensile strain in the lattice.

2.6. Infrared Spectra of Cu Solid Solution Doped TiO_2. Figure 4(a) indicates the infrared spectra of the Cu-doped TiO_2 samples. According to the electronegativity principle, the value of d_A was substituted into formula (3), and then, two kinds of stretching vibration frequencies of Ti-O in anatase were calculated: $\nu_{1A} = 622.76\,cm^{-1}$ and $\nu_{2A} = 511.62\,cm^{-1}$, and ν_A represents vibrational frequencies of the anatase. In the same way, the calculation results show that $\nu_{1R} = 1108.46\,cm^{-1}$, $\nu_{2R} = 1381.54\,cm^{-1}$, and ν_R represents vibrational frequency of the rutile. There were two strong absorption peaks: $3461.78\,cm^{-1}$ and $1658.74\,cm^{-1}$, which were caused by the H-Osw bond, H-Os bond, and H-Ow bond. s: Stretching vibration, w: bending vibration, Ti_A-O: Ti-O bond in anatase, and Ti_R-O: Ti-O bond in rutile. $Cu_A{}^i$-O: Cu atoms were incorporated in the interstitial anatase sites, $Cu_A{}^s$-O: Cu atoms replace Ti in the substitutional anatase sites, $Cu_R{}^i$-O: Cu atoms were incorporated in the interstitial rutile sites, and $Cu_R{}^s$-O: Cu atoms replace Ti in the substitutional rutile sites. The following data are obtained on the basis of the electronegativity principle. Figure 4(b) indicates that the absorption peaks of Ti_A-O, $Cu_A{}^s$-O, and $Cu_A{}^i$-O were similar. When the doping amount of Cu was 3 mol%, the absorption peaks of Ti_A-O were narrower. Meanwhile, the absorption peaks of $Cu_A{}^i$-O and $Cu_A{}^s$-O appear in the anatase lattice. Figure 4(c) indicates that when the doping amount of Cu was 5 mol%, the

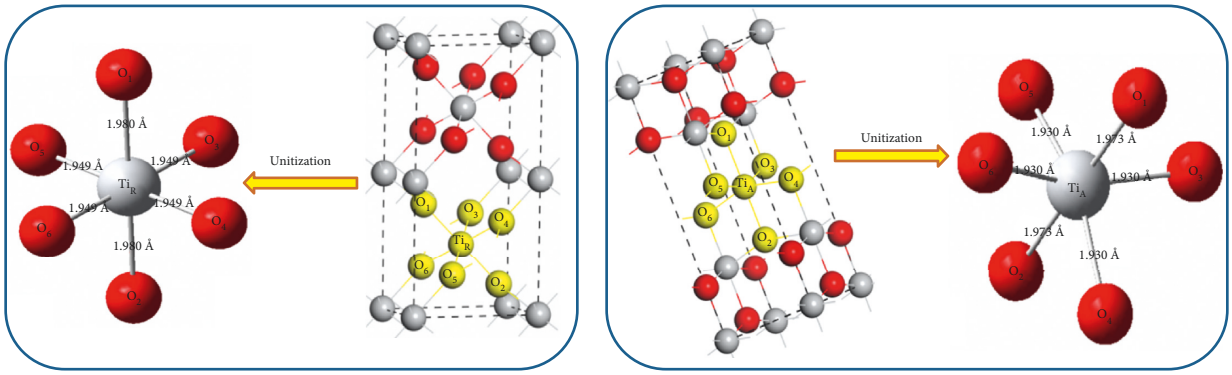

(a) (b)

Figure 1: The structural model of TiO_2: (a) the structural model of rutile and (b) the structural model of anatase.

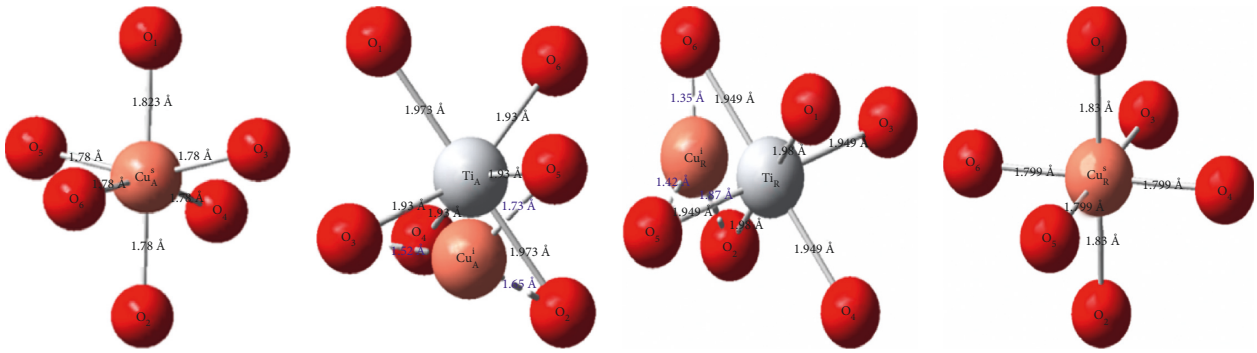

(a) (b) (c) (d)

Figure 2: Cu-doped TiO_2 structure model. (a) Cu replaces Ti atoms in the anatase; (b) Cu occupies in the anatase; (c) Cu replaces Ti atoms in the anatase; (d) Cu occupies in the anatase.

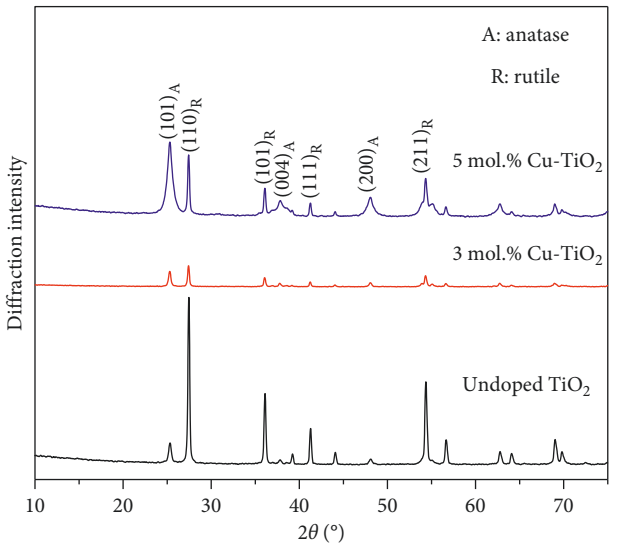

Figure 3: XRD patterns of the Cu-doped TiO_2 samples with different doping concentrations at calcination temperature (550°C).

absorption peaks of Cu_R^i-O and Cu_R^s-O appear in the rutile lattice. Transmissivity of the Cu-O bond decreased from $T = 0.74$ to $T = 0.38$. Meanwhile, the absorption peaks of Ti_R-O were also narrower. The results show that, in the rutile and anatase phases, a part of Cu and O atoms by interstitial solid solution to form Cu-O bond, and another part of Cu replaces Ti atoms by substitutional solid solution to form Cu-O bond with O atoms in the TiO_2 lattice. Cu_A^i-O: Cu atoms were incorporated in the interstitial anatase sites, Cu_A^s-O: Cu atoms replace Ti in the substitutional anatase sites, Cu_R^i-O: Cu atoms were incorporated in the interstitial rutile sites, and Cu_R^s-O: Cu atoms replace Ti in the substitutional rutile sites. The following data are obtained on the basis of the electronegativity principle. Figure 4(b) indicates that the absorption peaks of Ti_A-O, Cu_A^s-O, and Cu_A^i-O were similar. When the doping amount of Cu was 3 mol%, the absorption peaks of Ti_A-O were narrower. Meanwhile, the absorption peaks of Cu_A^i-O and Cu_A^s-O appear in the anatase lattice. Figure 4(c) indicates that when the doping amount of Cu was 5 mol%, the absorption peaks of Cu_R^i-O and Cu_R^s-O appear in rutile lattice. Transmissivity of the Cu-O bond decreased from $T = 0.74$ to $T = 0.38$. Meanwhile, the absorption peaks of Ti_R-O were also narrower. The results show that, in the rutile and anatase phases, O atoms in the TiO_2 lattice and some interstitial Cu atoms form Cu-O bond, and other substitutional Cu that replaces Ti atoms in TiO_2 lattice form the Cu-O bond with O atoms in the TiO_2 lattice.

Table 1: The lattice parameters of the Cu-doped TiO_2 samples with different doping concentrations.

	Anatase					Rutile					
Cu^{2+} (mol%)	d_{101} (Å)	d_{004} (Å)	d_{200} (Å)	$a = b$ (Å)	c (Å)	d_{101} (Å)	d_{101} (Å)	d_{101} (Å)	d_{101} (Å)	$a = b$ (Å)	c (Å)
0	3.517	2.373	1.891	3.782	9.493	3.741	2.869	2.481	1.784	4.594	2.953
3	3.516	2.374	1.893	3.787	9.497	3.744	2.865	2.487	1.787	4.597	2.956
5	3.514	2.376	1.894	3.785	9.496	3.743	2.861	2.482	1.788	4.596	2.957

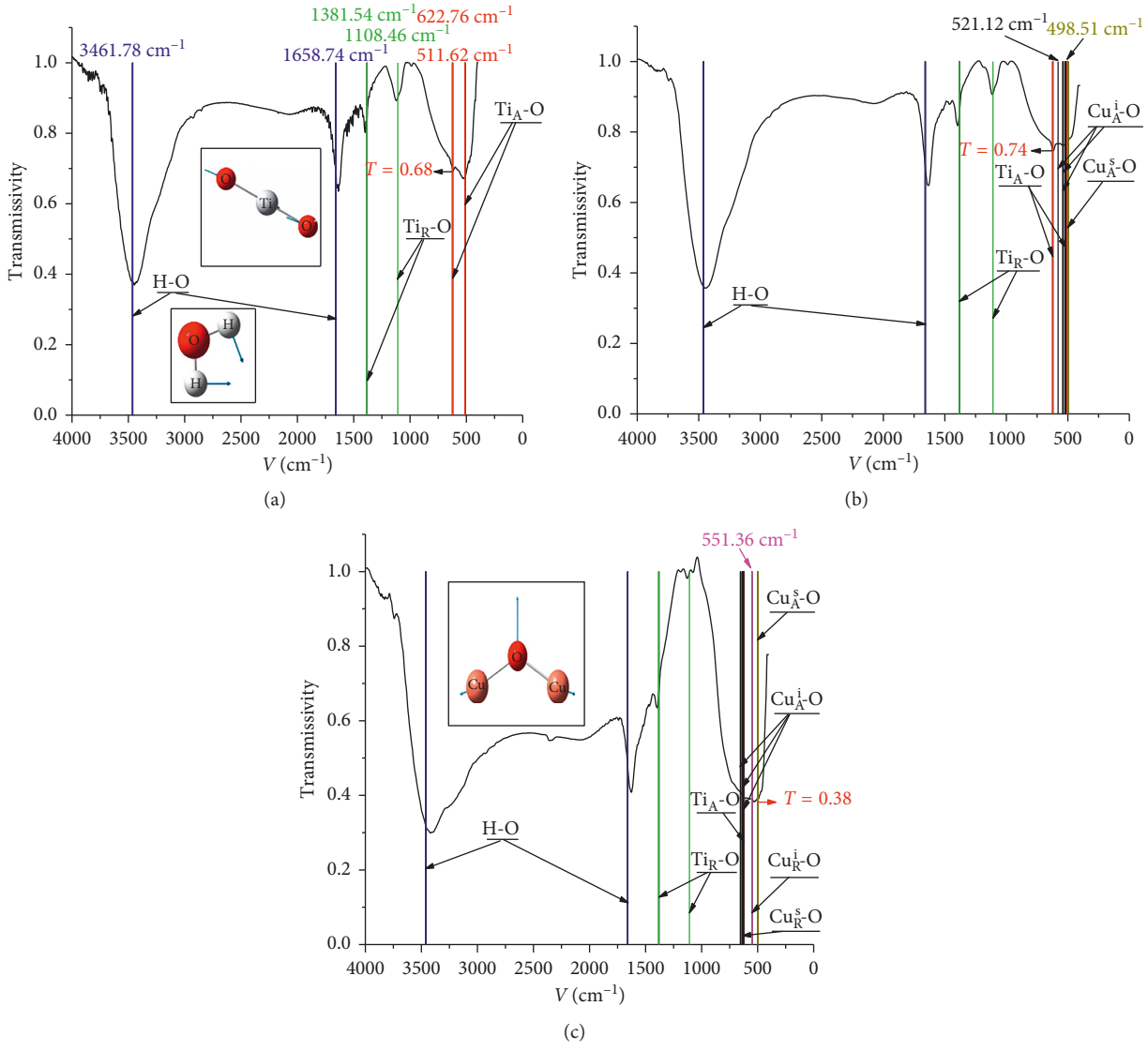

Figure 4: Infrared spectra of the Cu-doped TiO_2 samples with different doping concentrations at calcination temperature (550°C). (a) Undoped, (b) 3 mol% Cu, and (c) 5 mol% Cu.

3. Conclusion

The lattice parameters of samples calculated from the XRD patterns are shown in Table 1. The lattice parameters remain unchanged, independent of Cu^{2+} content. This is evident considering that a greater portion of the Cu^{2+} ions was well incorporated into the anatase and rutile TiO_2 lattice. When comparing to bulk anatase and rutile TiO_2, a small change of the lattice constant had been observed for the Cu-doped TiO_2 samples as shown in Table 1. According to Table 1, the changing of lattice constant is due to the tensile strain. It could be simulated by the principle of electronegativity that O atoms in the TiO_2 lattice and some interstitial Cu atoms form the Cu-O bond and other substitutional Cu that replaces Ti atoms in TiO_2 lattice form the Cu-O bond with O atoms in the TiO_2 lattice.

Data Availability

The lattice parameters of the Cu-doped TiO2 samples data used to support the findings of this study have been deposited in the ICDD repository (PDF #21-1272 and PDF #21-1276). The data of vibration frequency are calculated by ourselves.

Conflicts of Interest

The authors declare that they have no conflicts of interest.

Acknowledgments

This work was supported by the National Natural Science Foundation of China (Grant no. 51362017) and the plan of Yunnan Province Science and Technology Commission under Grant no. 2012ZE008. This work was also financially supported by Collaborative Innovation Fund Project of Precious Metals and Advanced Materials Innovation Center (Grant no. 14051708).

References

[1] M. Zeng, Y. Li, M. Mao, J. Bai, L. Ren, and X. Zhao, "Synergetic effect between photocatalysis on TiO_2 and thermocatalysis on CeO_2 for gas-phase oxidation of benzene on TiO_2/CeO_2 nanocomposites," *ACS Catalysis*, vol. 5, no. 6, pp. 3278–3286, 2015.

[2] R. Purbia, R. Borah, and S. Paria, "Carbon-doped mesoporous anatase TiO_2 multi-tubes nanostructures for highly improved visible light photocatalytic activity," *Inorganic Chemistry*, vol. 56, no. 16, pp. 10107–10116, 2017.

[3] K. Fujiwara, U. Müller, and S. E. Pratsinis, "Pd subnanoclusters on TiO_2 for solar-light removal of NO," *ACS Catalysis*, vol. 6, no. 3, pp. 1887–1893, 2016.

[4] D. M. Tobaldi, N. Rozman, M. Leoni et al., "Cu-TiO_2 hybrid nanoparticles exhibiting tunable photochromic behavior," *Journal of Physical Chemistry C*, vol. 119, no. 41, pp. 23658–23668, 2015.

[5] M. You, T. G. Kim, and Y. M. Sung, "Synthesis of Cu-doped TiO_2 Nanorods with various aspect ratios and dopant concentrations," *Crystal Growth and Design*, vol. 10, no. 2, pp. 983–987, 2010.

[6] J. M. Valero, S. Obregón, and G. Colón, "Active site considerations on the photocatalytic H_2 evolution performance of Cu-doped TiO_2 obtained by different doping methods," *ACS Catalysis*, vol. 4, no. 10, pp. 3320–3329, 2014.

[7] M. Liu, X. Qiu, M. Miyauchi, and K. Hashimoto, "Cu(II) oxide amorphous nanoclusters grafted Ti3+self-doped TiO_2: an efficient visible light photocatalyst," *Chemistry of Materials*, vol. 23, no. 23, pp. 5282–5286, 2011.

[8] K. I. Yamanaka, T. Ohwaki, and T. Morikawa, "Charge-carrier dynamics in Cu- or Fe-loaded nitrogen-doped TiO_2 powder studied by femtosecond diffuse reflectance spectroscopy," *Journal of Physical Chemistry C*, vol. 117, no. 32, pp. 16448–16456, 2013.

[9] J. Chen, G. Jiang, and T. Yuan, "Research on infrared spectra of (Fe, N) doped TiO_2 by the electronegativity principle," *Spectroscopy and Spectral Analysis*, vol. 37, no. 7, pp. 2305–2310, 2017.

[10] S. Shen, L. Zhao, Z. Zhou, and L. Guo, "Enhanced photocatalytic hydrogen evolution over Cu-doped $ZnIn_2S_4$ under visible light irradiation," *Journal of Physical Chemistry C*, vol. 112, no. 41, pp. 16148–16155, 2008.

[11] A. Sanchez-Soares and J. C. Greer, "A semimetal nanowire rectifier: balancing quantum confinement and surface electronegativity," *Nano Letters*, vol. 16, no. 12, pp. 7639–7644, 2016.

[12] M. B. Gordy and S. Willemann, "Constant proportion debt obligations: a postmortem analysis of rating models," *Management Science*, vol. 58, no. 3, pp. 476–492, 2012.

[13] C. C. Yang, Y. H. Yu, B. van der Linden, J. C. S. Wu, and G. Mul, "Artificial photosynthesis over crystalline TiO_2-based catalysts: fact or fiction?," *Journal of the American Chemical Society*, vol. 132, no. 24, pp. 8398–8406, 2010.

[14] R. Matheu, I. A. Moreno-Hernandez, X. Sala et al., "Photoelectrochemical behavior of a molecular Ru-based water-oxidation catalyst bound to TiO_2-protected Si photoanodes," *Journal of the American Chemical Society*, vol. 139, no. 33, pp. 11345–11348, 2017.